Cell Reports
Physical Science

CellPress
OPEN ACCESS

Article

Synthesis of microporous hydrogen-bonded supramolecular organic frameworks through guanosine self-assembly

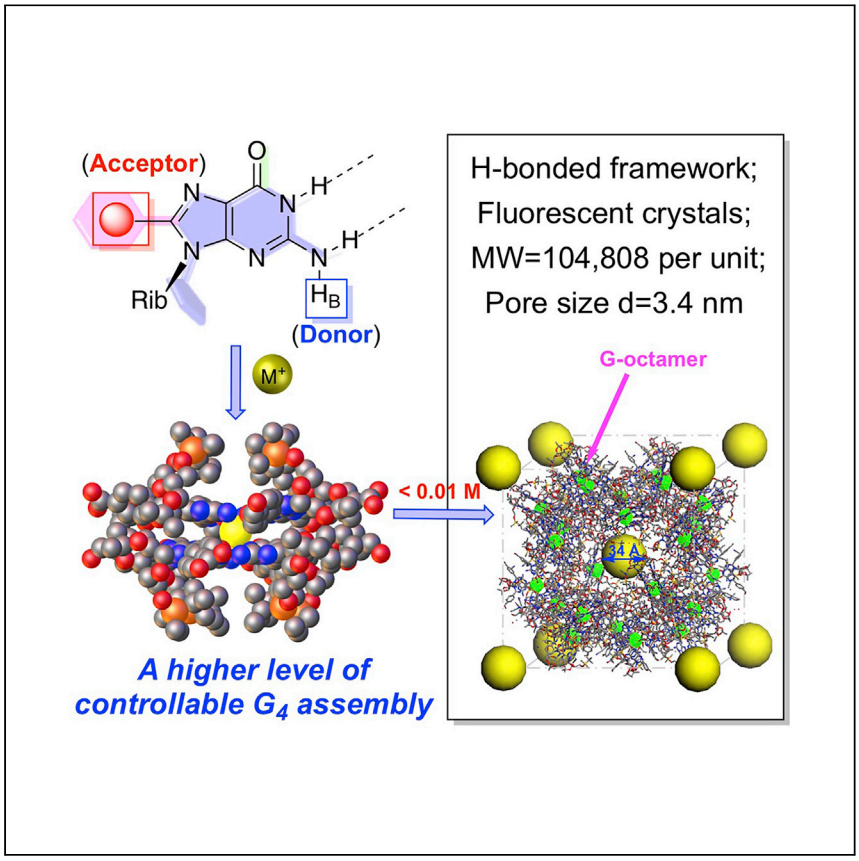

Extending the structural hierarchy and complexity through small-molecular self-assembly is interesting and challenging. He et al. achieved the synthesis of a non-covalent assembly with nanometer-size pores using a stable G-quadruplex as the building block, which opens an alternative avenue toward construction of three-dimensional, functional materials.

Ying He, Yanbin Zhang, Mengjia Liu, ..., Hao Guo, Aishun Ding, Xiaodong Shi

xmshi@usf.edu

Highlights

Hierarchical construction of molecular architecture through guanosine self-assembly

Well-defined supramolecular organic framework with inter-quadruplex interactions

Microporosity and strong fluorescence emission in blue-green region

He et al., Cell Reports Physical Science 2, 100519
August 18, 2021
https://doi.org/10.1016/j.xcrp.2021.100519

Cell Reports
Physical Science

CellPress
OPEN ACCESS

Article

Synthesis of microporous hydrogen-bonded supramolecular organic frameworks through guanosine self-assembly

Ying He,[1] Yanbin Zhang,[2] Mengjia Liu,[1] Kai Zhao,[1] Chuan Shan,[1] Lukasz Wojtas,[1] Hao Guo,[2] Aishun Ding,[2] and Xiaodong Shi[1,3,*]

SUMMARY

Extending the structural hierarchy and complexity through small-molecular self-assembly is a powerful way to obtain large discrete, functional molecular architecture. A hydrogen-bonded supramolecular organic framework (H_SOF) with nanometer-size pores is constructed in a solid state with simple guanosine-monomer self-assembly. To extend the hierarchy of the G-quartet self-assembly to a higher order than that of the traditional G-quadruplex, H-bond acceptors on the C-8 position of guanosine are introduced to establish inter-quadruplex linkage via H bonding to N(2)-H_B from the neighboring G-quartet. After screening different C-8 substitution groups and various synthesis conditions, H_SOF-G1a′ is obtained by solvent evaporation under diluted condition. Single-crystal X-ray structure reveals that cubic repeating units formed by G_8 are the supermolecule secondary building block (SBU) with large pores (d = 34 A). To our knowledge, this is the first G-quartet self-assembly with an organized structure beyond cylindrical G-quadruplexes.

INTRODUCTION

Among various supramolecular research directions, self-assembly is known for its ability to construct structures through designated building-block (small molecule) aggregation in a dynamic process.[1,2] Although self-assembly could facilitate the formation of large structures, a practical challenge is to achieve controllable structures with complexity.[3,4] As a dynamic assembly process, the resulting molecular structures from self-assembly heavily depend on the functionality of the basic building blocks. To reach structurally diverse molecular architectures, integration of various non-covalent interaction sites into one building block is necessary and often requires good binding-mode compatibility. Thus, a system that could increase supramolecular complexity from simple building blocks (extending structural hierarchy) is intriguing for both fundamental supramolecular research and practical applications.

Guanosine is one unique supramolecular building block with embedded H-bond donors and acceptors (Figure 1A).[5–7] The 90° angle between H-bond donors and acceptors leads to the formation of square planar G-quartets.[8–10] Four central oxygens of the G-quartet can bind with alkali or alkali earth metal cations through ion-dipole interactions to stabilize the G-quartet. The G-quadruplexes are formed through the stacking of G_4-plane in a sandwich manner. Until now, these were the known assembly interactions, which made guanosine a very interesting supramolecular system with hierarchical assembly ability.

Our interest in pursuing guanine-based H-bonded "molecular architecture" was initiated by our recent success in achieving stable and well-defined G-octamers.[11]

[1]Department of Chemistry, University of South Florida, 4202 E. Fowler Avenue, Tampa, FL 33620, USA

[2]Department of Chemistry, Fudan University, 2005 Songhu Road, Shanghai 200438, PR China

[3]Lead contact

*Correspondence: xmshi@usf.edu

https://doi.org/10.1016/j.xcrp.2021.100519

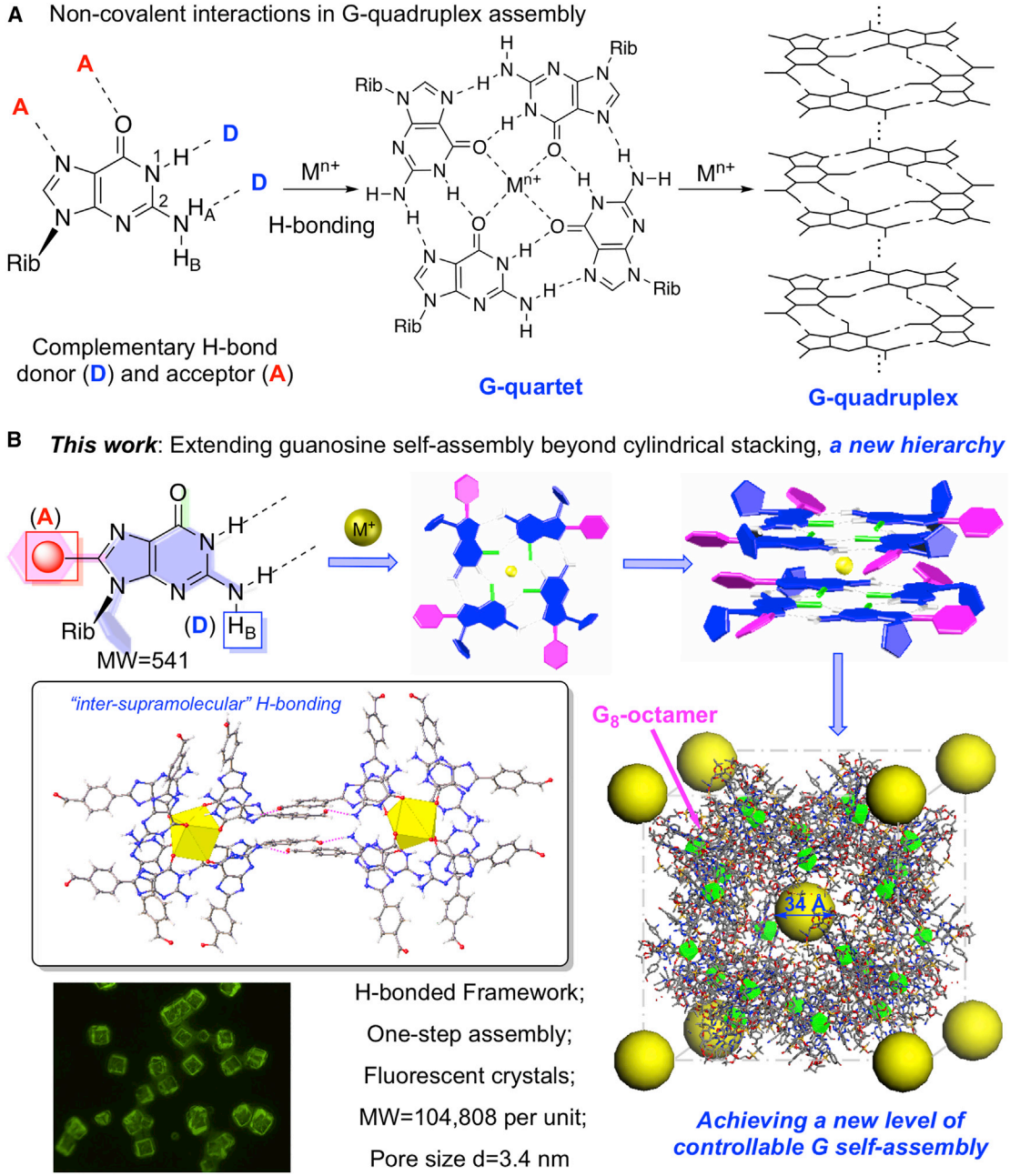

Figure 1. Hierarchical guanosine self-assembly through ligand design

(A) Non-covalent interactions in the G-quadruplex assembly, including H-bonding, ion-dipole interactions, and G-quartet stacking.

(B) This work: extending the G-quartet self-assembly beyond cylindrical stacking.

It has been reported that external parameters, such as solvent polarity, cations, and anions have shown decisive roles in regulating the precise guanosine self-assembly into discrete G-quadruplex formations.[12,13] However, controlling G-quartet stacking is a challenging task with only a few successful examples reported,[14,15] which is mainly because of the equilibrium between various "stacking species" in solution. This has limited the potential of further extending the assembly into the next level, in which a well-defined G-quadruplex is crucial as the building unit.[16] Recently, through the introduction of bulky groups on both C8 aryl and ribose

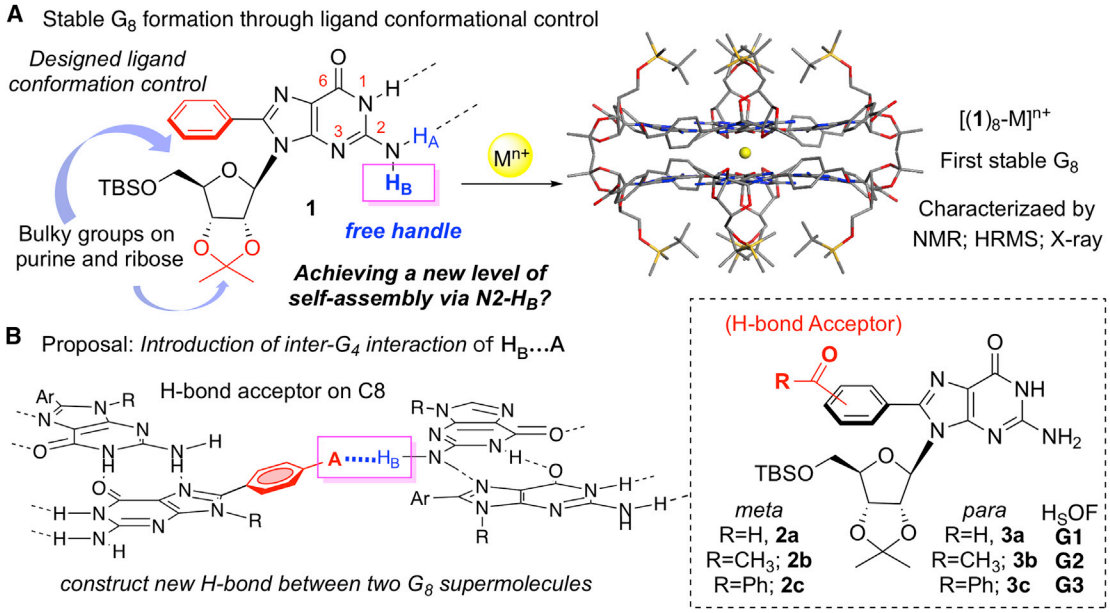

Figure 2. Extending guanosine self-assembly via ligand design

(A) Stable G_8 formation through ligand conformational control.

(B) Proposal: introduction of an inter-G_4 interaction of $H_B \cdots A$.

(2′,3′-isopropylidene), we developed a conformational control strategy for precise formations of discrete and stable G-octamers in both solution and solid states for the first time (Figure 2A).[11,17]

In this work, we report the successful extension of a G_4 assembly through the introduction of H-bond interactions between different G-quadruplexes, achieving H_sOF cubes with nano-sized pores (Figure 1B). To our knowledge, this is the first example of well-defined G-quartet self-assembly with inter-quadruplex interactions in the solid state.

RESULTS AND DISCUSSION

Self-assembling study of guanosine derivatives with KPF_6

To pursue a greater level of guanosine self-assembly from simple building blocks, it is important to use all available functional moieties for the overall aggregation. As shown in the G_4 structures, N(2)–H_A is a critical H-bond donor for the G-quartet formation (untouchable). The "free" N(2)-H_B is the potential "handle" for the introduction of functionality. Some N2-modified guanosine derivatives have been previously reported in the literature through the introductions of alkyl and acetyl groups on the N2 position. However, rather complex self-assembly mixtures were observed in all those cases. This not only suggests the importance of keeping N(2)-H_B un-protected for stable and discrete G_4 formation but also highlights the challenges in "upgrading" supramolecular aggregation into a higher-order assembly. Considering that N(2)-H_B is a potential H-bond donor,[14,18–20] we postulate that introduction of H-bond acceptor on the C8-aryl might provide the additional H-bonding interactions between G-quartets to further extend the overall assembly into a higher level. (Figure 2B) Our design is to apply structurally well-defined G-octamer as the secondary building block (SBU) for the construction of larger molecular architectures through "inter-supramolecular" interactions. Based on that idea, meta- (**2a–2c**) and para- (**3a–3c**) substituted ketone/aldehydes were prepared (see Supplemental experimental procedures for synthetic procedures

and Figures S1–S12 for NMR spectra) and applied for the self-assembly studies in an organic solution. Based on previous binding studies,[11,21] KPF_6 was selected as the ion pair for the G-quadruplex construction because of its strong cation binding and non-coordinating anion.

Similar to 8-phenyl-substituted ligand **1**, one set of ^{1}H NMR signals was observed when treating these G-ligands (**2a–2c**, **3a–3c**) with KPF_6 in $CDCl_3$, suggesting the formation of G-octamers (see Figure S13). This result is encouraging because it confirmed that the introduction of H-bond receptor on the C8-aryl group is compatible with a G_4 formation, which sets up the foundation for the proposed G_8–G_8 inter-quadruplex interactions. According to our previous study,[11] the meta-carbonyl-substituted ligand **2b** led to a cross-layer H-bonded G-octamer (confirmed by X-ray). Although it did not provide the desired G_8–G_8 interaction, that result greatly supported our proposal to use N(2)-H_B as the additional H-bond donor handle without interrupting the G-quartet formation. Encouraged by this result, we put our attention to the para-substituted analogous **3**. Compared with the meta-substituted ligand **2**, in which the carbonyl group is tilted for cross-layer H-bond interaction, the carbonyl groups in para-substituted ligand **3** are positioned perpendicular to the stacking quartets, allowing possible inter-quartet interactions.

Low-temperature ^{1}H NMR experiments were first performed to examine the possibility of this extra H-bonding. Notably, although N(2)-H_A forms an H-bond as part of the G-quartet, the two NH_2 protons are interconvertible. Therefore, the NH_2 protons of complex $[(\mathbf{1})_8\text{-K}]^+$ do not appear in ^{1}H NMR at room temperature because of the fast exchange at NMR timescales. Cooling the sample to −20°C provides the NH_2 protons two separated broad signals (see Supplemental information; H_A, 10.28 ppm; H_B, 5.89 ppm). In comparison, conducting variable temperature (VT)-NMR experiments with G_8 complexes from para-carbonyl ligand **3a–3c**, the NH_2 protons start to show up at 0°C, suggesting the formation of additional H-bonds that lock the NH_2 exchange, as expected (see Figures S14 and S15).

Although the VT ^{1}H NMR results suggested the possibility of forming additional H-bond with N(2)-H_B, the overall interactions are not strong enough to produce stable polymeric complexes in solution at room temperature. This is likely due to the decrease in entropy associated with the formation of highly ordered molecular architecture. Crystal engineering[22] can be applied as a potential solution for the construction of large molecular architecture in the solid state by avoiding the unfavored entropy effect in solution. The three complexes of $[(\mathbf{3})_8\text{-K}]^+PF_6^-$ were applied to grow solid crystals under various conditions. Fortunately, the crystal structures of $[(\mathbf{3a})_8\text{-K}]^+PF_6^-$ were successfully obtained as shown in Figure 3A.[19] Ketone **3b** failed to form a stable crystal for structural determination under the current conditions. Although obtaining the crystal data of $[(\mathbf{3c})_8\text{-K}]^+PF_6^-$ was not successful, the crystal structure of $[(\mathbf{3c})_8\text{Na}]^+$ was later confirmed with CO_3^{2-} as the counter anion (Figure 3B). Notably, in both cases, no anion binding was observed by X-ray, confirming that the overall molecular architectures are controlled by ligand and cation.

Single-crystal structure analysis of H_5OF-G1a and H_5OF-G3

Single-crystal X-ray diffraction revealed the packing of G-octamer for yellow block-shaped crystals **H_5OF-G1a** (from **3a**) with little porosity. Each G-octamer forms an H-bond with four adjacent G_8-adopting tetrahedron geometry (see Supplemental information for details; Figures S16–S18). The resulting three-dimensional (3D) network can be symbolized as a dia net. This compact knitting-like topology with

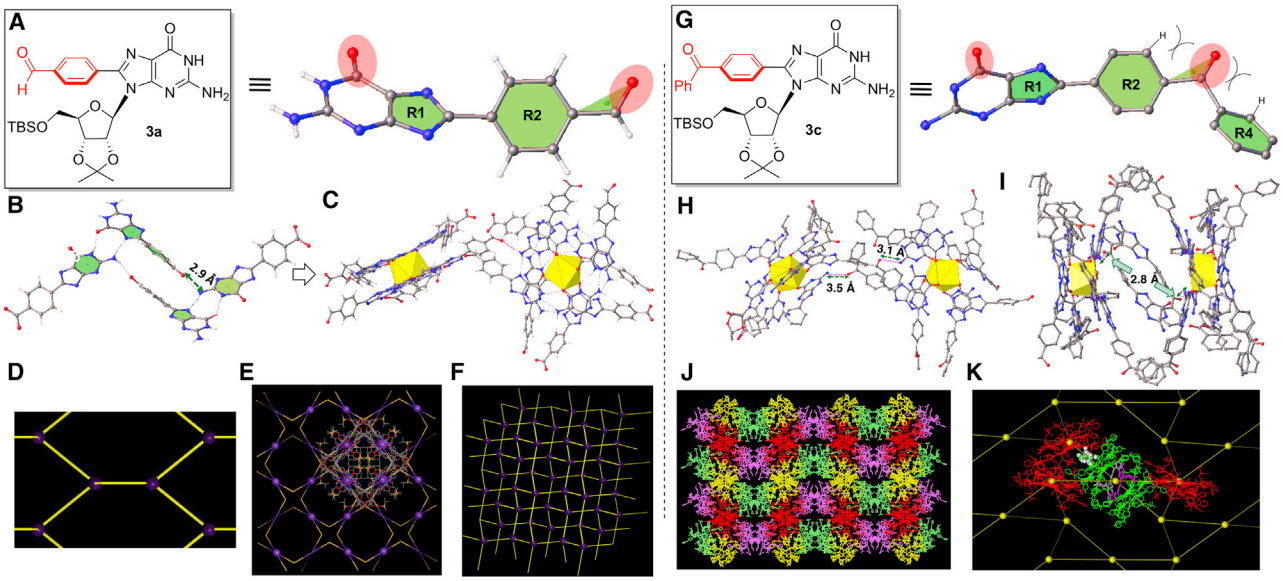

Figure 3. X-ray crystal structures of H_5OF-G1a and H_5OF-G3

(A) Conformation of guanosine **3a** in **H_5OF-G1a**.

(B) Cross-G_4 H-bonding.

(C) G_8–G_8 inter-quartet interaction.

(D) Connectivity between G_8 in **H_5OF-G1a**. Each purple sphere ball represents one G_8.

(E) Packing of **H_5OF-G1a** from the c axis.

(F) Simplified single-net structure of **H_5OF-G1a** showing the dia topology.

(G) Conformation of guanosine **3c** in **H_5OF-G3**.

(H) G_8–G_8 interactions in **H_5OF-G3**.

(I) H-bonding between monomeric guanosine **3c** and G_8.

(J) Packing of **H_5OF-G3** from the a axis. Four G_8 in an asymmetric unit shown in red, green, yellow, and purple.

(K) Simplified single-net structure of **H_5OF-G3** showing cross-G_8 H-bonding (between red and green) and C-H$\cdots\pi$ weak interactions (between the tert-butyldimethylsilyl group and guanine). Two monomeric **3c** (gray and pink) are in the cavity of green G_8. Each forms two H-bonding with the adjacent G_8 in green.

G_8 as the knot extends in four directions. Each G_8 has inter-G_4 H-bonding with the G_8 of four other G_8 neighbors. The lack of porosity could be accounted for by ribose and silyl groups, which takes up space in the cavity (Figure 3E). The **H_5OF-G3** (from **3c** and Na^+) showed similar inter-G_8 H-bonding, as expected (See Table S4 for detailed crystal data and structure refinement). Four different $[(\mathbf{3c})_8Na]^+$ SBUs were identified in an asymmetric unit (Figure 3J). As shown in Figure 3H, two pairs of N(2)-$H_B\cdots$O H-bond were observed (one between the green and red G_8 units and one between purple and yellow G_8 units). Because of the steric repulsion between arene rings (R2 versus R4), the C=O group is not planar to either phenyl ring, which likely accounts for the weaker H-bond interactions (Figure S19). Notably, two monomeric **3c** units are found located in the cavity formed by two G_8 units (Figure 3I). Each forms two H-bonding with an adjacent G_8. Abstracting the structure by two pairs of G_8 dimers separately produced two raffled layers (see Figure S20). The two layers complement each other like the zipper to support the framework (see simplified net in Figure S21). In addition, weak C–H$\cdots\pi$ interactions between the TBS group and the guanine were observed within and between layers (see Figure S22). Because of the compact packing, bulky TBS groups and monomeric **3c** blocking the gaps between G_8 units, no pore was observed for **H_5OF-G3**.

The two **H_5OF** crystal structures are exciting because they confirmed the possibility of using G_8 as the SBU to construct further extended supramolecular architectures.

In addition to the two crystalline materials, we wondered whether we could extend the H_SOF synthesis and apply that supramolecular crystal engineering process for the construction of highly ordered porous materials.

Porous H_SOF synthesis from crystallization of $[(3a)_8\text{-}K]^+PF_6^-$

Notably, porous organic frameworks have attracted increasing attentions in materials science over the past decades.[23–30] It was widely explored in gas adsorption,[24,28,31] gas separation,[25,32–34] catalysis,[35–44] drug delivery,[45,46] among other fields.[47–54] Formed by non-covalent interactions and intermolecular H-bonded subunits, HOFs (hydrogen-bonded organic frameworks) have emerged as an intriguing class of porous frameworks.[27,55–64] Compared with metal-organic frameworks (MOFs) and covalent organic frameworks (COFs), H_SOFs feature high crystallinity, solution processability, easy healing, and regeneration ability.[63–70] However, because of the labile nature of H-bonding, successful examples of this type of porous materials are relatively rare.

Considering that different frameworks are under equilibrium in solution, their solubility could vary under different solvent systems. Comparing the two H_SOFs shown in Figure 3, the porous H_SOFs with larger structures per unit cell will likely have significantly reduced solubility and should be crystallized out of the system earlier, if giving sufficient time to reach an equilibrium. In the past, when preparing typical G_8-complex crystals, a relatively high concentration was usually applied to reach a supersaturation point in a comparatively short time (upon solvent evaporation). However, that might not be ideal for the synthesis of porous H_SOFs because the packed H_SOF might be the dominant supermolecules presented in solution at that greater concentration. With that concern in mind, we performed a different crystal synthesis using the same G_8-octamers from ligand **3** under various diluting conditions. To our great pleasure, a different shape of crystals was generated with $[(\mathbf{3a})_8\text{-}K]^+PF_6^-$ when treating the G_8-octamer under significantly diluted conditions with an initial concentration <0.01 M. The X-ray crystal structure of that H_SOF was successfully determined as shown in Figure 3. It is noteworthy that this crystal synthesis process is very robust and has been successfully repeated for more than 20 times. The resulting crystalline materials have been successfully synthesized at >500-mg scale.

Single-crystal structure analysis of H_SOF-G1a′

As expected, this transparent crystal (**H_SOF-G1a′**) in the rectangle prism shape (significantly different from the crystal of **H_SOF-G1a**) unveiled a structure with inter-quadruplex H-bonding. (See Table S5 for detailed crystal data and structure refinement) The whole structure is highly porous, with a calculated diameter about 34 Å (Figure S23) The pore space within in the frameworks encapsulate some acetonitrile-solvent molecules. Each unit cell is composed of 24 G_8s (green sphere ball) as the SBU. As shown in Figure 4A, the simplified net demonstrated helical structures along the c axis. The helix is formed by G_8 interactions. To demonstrate the connectivity between G_8s, the view from a diagonal of the cubic structure was taken (Figure 4B). Using this kaleidoscope-like shape, three types of connectivity (G_8–G_8 interaction) were identified: (1) node A in a blue triangle formed by six G_8s; (2) a vertex of three triangles connecting in C_3 symmetry, which leads to node B as the center of the three G_8s; (3) an extension of the lines from the triangle results in a crossing, which represents node C (see Figures S24–S28). Nodes A and B are composed of dimeric G_8 as shown in Figure 4B. Each G_8 provides a formyl group on C8-aryl as the H-bond donor to interact with N(2)-H_B on the other G_8s through four cross-G_4 H-bonding. On the other hand, a trimeric G_8–G_8 interaction was observed for node C, in which six cross-G_4 H-bonds were formed. By abstracting and connecting those three nodes

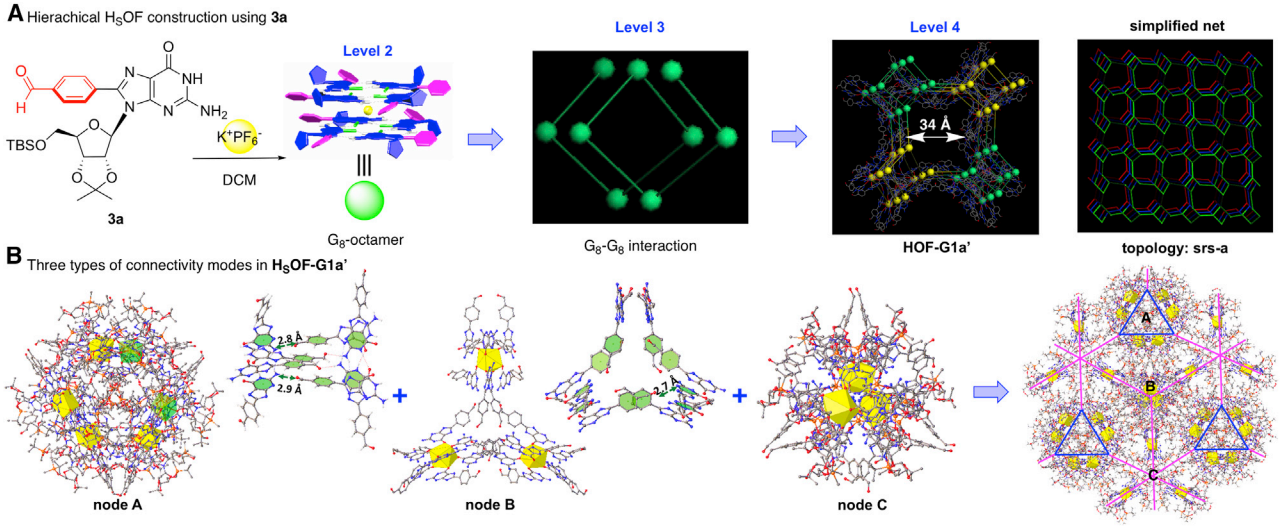

Figure 4. Hierarchical construction and crystal structure of H_SOF-G1a′ from 3a

(A) Hierarchical construction of **H_SOF-G1a′** from **3a**. Level 2: formation of G_8 using C8-functionalized guanosine derivatives **3a**. Level 3: G_8–G_8 interaction and connectivity. Each green sphere ball represents one G_8. Level 3: packing of **H_SOF-G1a′** from a/b/c axes.

(B) Three types of connectivity from diagonal view in **H_SOF-G1a′** structure.

into a simplified, interpenetrated structure, a topology of the underlying net of srs-a (3/3/C1) was revealed. Compared with **H_SOF-G1a** and **H_SOF-G3**, G_8–G_8 interactions of **H_SOF-G1a′** are in nearer (H-bond distance: 2.7 A versus 3.5 A), and more cross-G_4 H-bonds were formed. In addition, three different modes of connectivity support are needed to facilitate the 3D cubic architecture. In contrast, interactions among G_8 in **H_SOF-G3** is loose, likely because of the bulky phenyl group inserted into the vacancy of the adjacent G_8, which hindered further support of the assembly in the c axis. Consequently, simple overlaying of layers with a weak interaction was adopted in **H_SOF-G3**, resulting in a non-porous structure. This result indicates the steric effect of carbonyl substitution on the G_8–G_8 interaction geometry, which further influences the entire organic architecture. (see Figure S29 and Table S1)

Gas sorption and photoluminescence properties of the porous H_SOF-G3

To explore the property and functionality of this H_SOF structure, powder X-ray diffraction (PXRD) patterns were collected, and the phase purity was confirmed using the freshly grown crystalline sample. The diffraction pattern of **H_SOF-G1a′** is consistent with the calculated data from its X-ray single-crystal structure (see Figure S30). To investigate the gas sorption capacity of the synthesized H_SOF materials, N_2 adsorption data were collected at 77 K to examine the porosity of activated **H_SOF-G1a′** (see Note S1 and Figure S31). The adsorption plot shows a reversible type-I isotherm, which is characteristic for porous materials with a steep increase at P/P_0 = 0.2. It provides the maximum N_2 uptake of 30 $cm^3\ g^{-1}$ at P/P_0 = 0.99. The results were employed to estimate their surface areas. Fitting the adsorption isotherms of CO_2 to the Brunauer-Emmett-Teller (BET) equation provides a surface area of ~100 $m^2\ g^{-1}$ (Langmuir surface area: ~115 $m^2\ g^{-1}$). The small value for the surface area is likely due to framework change when the guest molecule was removed during the activation process. Furthermore, a total pore volume of 0.046 $cm^3\ g^{-1}$ was estimated using the Horvath-Kawazoe equation (see Figure S32, Table S2, and Note S2).

With the intrinsic, strong fluorescence emission of the G-octamer complexes, it will be interesting to explore whether the H_SOF material inherits the fluorescence

activity. The photoluminescent properties of H_SOF samples were evaluated in comparison with the G_8 complexes in a solid state (see Figures S33 and S34, Table S3, and Note S3 for details). All the G-complex samples exhibited some red-shift emission compared with that of monomeric **3a**, **3b**, and **3c**, respectively. **H_SOF-G1a′** demonstrated significantly enhanced emission intensity compared with that of monomeric **3a** and $[(\mathbf{3a})_8\text{-K}]^+PF_6^-$ complex with a slight blue-shift emission. Further applications using the fluorescent porous H_SOF in organic molecule absorption[71,72] and detection[73,74] are currently underway in our laboratory.

In conclusion, through the controllable stacking, the G-octamer system can serve as a scaffold in higher-order molecular self-assembly processes. Hierarchical construction of a H_SOF through C8-aryl guanosine self-assemblies was achieved. A dramatic increase in molecular weight from 541 g/mol to 104,808 g/mol per unit cell was readily realized, indicating a robust capability and the advantage of a supramolecular assembly in producing complicated molecular architectures. Microporosity for potential gas sorption and small-molecule absorption was observed. Furthermore, the strong fluorescence emission in the blue-green region demonstrated its potentials as bioprobes. The concept of using a stable G_8 as the SBU for extended self-assembly opens an alternative avenue toward construction of 3D functional materials.

EXPERIMENTAL PROCEDURES

Resource availability

Lead contact

Further information and requests for resources should be directed to, and will be fulfilled by, the lead contact, Xiaodong Shi (xmshi@usf.edu).

Materials availability

All unique/stable reagents generated in this study are available from the lead contact with a completed materials transfer agreement.

Data and code availability

The authors declare that the data supporting the findings of this study are available within the article and the Supplemental information. All other data are available from the lead contact upon reasonable request. The accession numbers for the crystallographic dataset reported in this paper for **H_SOF-G3** and **H_SOF-G1a′** are Cambridge Crystallographic Data Centre (CCDC): 2077670, 2077671.

SUPPLEMENTAL INFORMATION

Supplemental information can be found online at https://doi.org/10.1016/j.xcrp.2021.100519.

ACKNOWLEDGMENTS

We are grateful to the NSF (CHE-1665122) and NIH (1R01GM120240-01) for financial support. We thank Evgeniya (Jenya) Semenova and Professor Alex Grenning (University of Florida) for assistance in conducting the VT-NMR experiments. This work has been supported in part by the University of South Florida Interdisciplinary NMR Facility and the Chemical Purification, Analysis, and Screening (CPAS) core facility. This work is dedicated to the 100th anniversary of Chemistry at Nankai University.

AUTHOR CONTRIBUTIONS

Y.H. conducted the experiments, performed the characterization, and analyzed the results and data; Y.Z. conducted gas sorption experiments; Y.H. and M.L. carried out

the material synthesis; K.Z. drew the crystal structures; C.S. collected the crystal data; L.W. solved and refined the crystal structures; X.S. conceived the original idea, set research directions, and designed the experiments; and X.S., H.G., and A.D. supervised the research.

DECLARATION OF INTERESTS

The authors declare no competing interests.

Received: May 11, 2021
Revised: May 27, 2021
Accepted: July 7, 2021
Published: July 29, 2021

REFERENCES

1. Zeng, F., and Zimmerman, S.C. (1997). Dendrimers in supramolecular chemistry: from molecular recognition to self-assembly. Chem. Rev. *97*, 1681–1712.

2. Chen, G., and Jiang, M. (2011). Cyclodextrin-based inclusion complexation bridging supramolecular chemistry and macromolecular self-assembly. Chem. Soc. Rev. *40*, 2254–2266.

3. Yuan, Z., Zhao, C., Di, Z., Wang, W.-X., and Lai, Y.-C. (2013). Exact controllability of complex networks. Nat. Commun. *4*, 2447.

4. Xia, Y., Yin, Y., Lu, Y., and McLellan, J. (2003). Template-assisted self-assembly of spherical colloids into complex and controllable structures. Adv. Funct. Mater. *13*, 907–918.

5. Phan, A.T. (2010). Human telomeric G-quadruplex: structures of DNA and RNA sequences. FEBS J. *277*, 1107–1117.

6. Mamajanov, I., Engelhart, A.E., Bean, H.D., and Hud, N.V. (2010). DNA and RNA in anhydrous media: duplex, triplex, and G-quadruplex secondary structures in a deep eutectic solvent. Angew. Chem. Int. Ed. Engl. *49*, 6310–6314.

7. Biffi, G., Di Antonio, M., Tannahill, D., and Balasubramanian, S. (2014). Visualization and selective chemical targeting of RNA G-quadruplex structures in the cytoplasm of human cells. Nat. Chem. *6*, 75–80.

8. Sessler, J.L., Sathiosatham, M., Doerr, K., Lynch, V., and Abboud, K.A. (2000). A G-quartet formed in the absence of a templating metal cation: a new 8-(*N*,*N*-dimethylaniline) guanosine derivative. Angew. Chem. Int. Ed. Engl. *39*, 1300–1303.

9. Sessler, J.L., Jayawickramarajah, J., Sathiosatham, M., Sherman, C.L., and Brodbelt, J.S. (2003). Novel guanosine-cytidine dinucleoside that self-assembles into a trimeric supramolecule. Org. Lett. *5*, 2627–2630.

10. Gottarelli, G., Masiero, S., Mezzina, E., Pieraccini, S., Rabe, J.P., Samorí, P., and Spada, G.P. (2000). The self-assembly of lipophilic guanosine derivatives in solution and on solid surfaces. Chemistry *6*, 3242–3248.

11. He, Y., Zhang, Y., Wojtas, L., Akhmedov, N.G., Thai, D., Wang, H., Li, X., Guo, H., and Shi, X. (2019). Construction of a cross-layer linked G-octamer *via* conformational control: a stable G-quadruplex in H-bond competitive solvents. Chem. Sci. (Camb.) *10*, 4192–4199.

12. González-Rodríguez, D., van Dongen, J.L.J., Lutz, M., Spek, A.L., Schenning, A.P.H.J., and Meijer, E.W. (2009). G-quadruplex self-assembly regulated by Coulombic interactions. Nat. Chem. *1*, 151–155.

13. Liu, M., He, Y., Shan, C., Wojtas, L., Ghiviriga, I., Fathalla, O., Yan, Y., Li, X., and Shi, X. (2021). Anion mediated, tunable isoguanosine self-assemblies: decoding the conformation influence and solvent effects. Chem. Sci. (Camb.) *12*, 7569–7574.

14. Shi, X., Mullaugh, K.M., Fettinger, J.C., Jiang, Y., Hofstadler, S.A., and Davis, J.T. (2003). Lipophilic G-quadruplexes are self-assembled ion pair receptors, and the bound anion modulates the kinetic stability of these complexes. J. Am. Chem. Soc. *125*, 10830–10841.

15. Martín-Hidalgo, M., and Rivera, J.M. (2011). Metallo-responsive switching between hexadecameric and octameric supramolecular G-quadruplexes. Chem. Commun. (Camb.) *47*, 12485–12487.

16. Li, X., Sánchez-Ferrer, A., Bagnani, M., Adamcik, J., Azzari, P., Hao, J., Song, A., Liu, H., and Mezzenga, R. (2020). Metal ions confinement defines the architecture of G-quartet, G-quadruplex fibrils and their assembly into nematic tactoids. Proc. Natl. Acad. Sci. USA *117*, 9832–9839.

17. He, Y., Zhang, Y., Wojtas, L., Akhmedov, N.G., Pan, Q., Guo, H., and Shi, X. (2020). Reversed cation selectivity of G_8-octamer and G_{16}-hexadecamer towards monovalent and divalent cations. Chem. Asian J. *15*, 1030–1034.

18. Shi, X., Fettinger, J.C., and Davis, J.T. (2001). Homochiral G-quadruplexes with Ba^{2+} but not with K^{+}: the cation programs enantiomeric self-recognition. J. Am. Chem. Soc. *123*, 6738–6739.

19. Shi, X., Fettinger, J.C., and Davis, J.T. (2001). Ion-pair recognition by nucleoside self-assembly: guanosine hexadecamers bind cations and anions. Angew. Chem. Int. Ed. *40*, 2827–2831.

20. García-Arriaga, M., Hobley, G., and Rivera, J.M. (2008). Isostructural self-assembly of 2′-deoxyguanosine derivatives in aqueous and organic media. J. Am. Chem. Soc. *130*, 10492–10493.

21. Zhang, Y., He, Y., Wojtas, L., Shi, X., and Guo, H. (2020). Construction of supramolecular organogel with circularly polarized luminescence by self-assembled guanosine octamer. Cell Rep. Phys. Sci. *1*, 100211.

22. Corpinot, M.K., and Bučar, D.-K. (2019). A practical guide to the design of molecular crystals. Cryst. Growth Des. *19*, 1426–1453.

23. Zhou, H.C., and Kitagawa, S. (2014). Metal-organic frameworks (MOFs). Chem. Soc. Rev. *43*, 5415–5418.

24. Getman, R.B., Bae, Y.-S., Wilmer, C.E., and Snurr, R.Q. (2012). Review and analysis of molecular simulations of methane, hydrogen, and acetylene storage in metal-organic frameworks. Chem. Rev. *112*, 703–723.

25. Lin, R.-B., Xiang, S., Xing, H., Zhou, W., and Chen, B. (2019). Exploration of porous metal-organic frameworks for gas separation and purification. Coord. Chem. Rev. *378*, 87–103.

26. James, S.L. (2003). Metal-organic frameworks. Chem. Soc. Rev. *32*, 276–288.

27. Ding, S.-Y., and Wang, W. (2013). Covalent organic frameworks (COFs): from design to applications. Chem. Soc. Rev. *42*, 548–568.

28. Li, J.-R., Kuppler, R.J., and Zhou, H.-C. (2009). Selective gas adsorption and separation in metal-organic frameworks. Chem. Soc. Rev. *38*, 1477–1504.

29. Ma, L., Abney, C., and Lin, W. (2009). Enantioselective catalysis with homochiral metal-organic frameworks. Chem. Soc. Rev. *38*, 1248–1256.

30. Feng, L., Wang, K.-Y., Lv, X.-L., Yan, T.-H., and Zhou, H.-C. (2020). Hierarchically porous metal-organic frameworks: synthetic strategies and applications. Natl. Sci. Rev. *7*, 1743–1758.

31. Liu, J., Thallapally, P.K., McGrail, B.P., Brown, D.R., and Liu, J. (2012). Progress in adsorption-

based CO_2 capture by metal-organic frameworks. Chem. Soc. Rev. *41*, 2308–2322.

32. Khan, N.A., Hasan, Z., and Jhung, S.H. (2013). Adsorptive removal of hazardous materials using metal-organic frameworks (MOFs): a review. J. Hazard. Mater. *244-245*, 444–456.

33. Li, J.-R., Ma, Y., McCarthy, M.C., Sculley, J., Yu, J., Jeong, H.-K., Balbuena, P.B., and Zhou, H.-C. (2011). Carbon dioxide capture-related gas adsorption and separation in metal-organic frameworks. Coord. Chem. Rev. *255*, 1791–1823.

34. Banerjee, D., Simon, C.M., Elsaidi, S.K., Haranczyk, M., and Thallapally, P.K. (2018). Xenon gas separation and storage using metal-organic frameworks. Chem *4*, 466–494.

35. Liang, J., Huang, Y.-B., and Cao, R. (2019). Metal–organic frameworks and porous organic polymers for sustainable fixation of carbon dioxide into cyclic carbonates. Coord. Chem. Rev. *378*, 32–65.

36. Zhao, K., He, Y., Shan, C., Ren, J., Wojtas, L., Wang, L., Li, G., Song, Z., and Shi, X. (2020). "Orthogonal-twisted-arm" ligands for the construction of metal-organic frameworks: new topology and catalytic reactivity. Chemistry *26*, 16272–16276.

37. Ji, P., Feng, X., Oliveres, P., Li, Z., Murakami, A., Wang, C., and Lin, W. (2019). Strongly Lewis acidic metal-organic frameworks for continuous flow catalysis. J. Am. Chem. Soc. *141*, 14878–14888.

38. Yan, S., Guan, X., Li, H., Li, D., Xue, M., Yan, Y., Valtchev, V., Qiu, S., and Fang, Q. (2019). Three-dimensional Salphen-based covalent-organic frameworks as catalytic antioxidants. J. Am. Chem. Soc. *141*, 2920–2924.

39. Xu, C., Fang, R., Luque, R., Chen, L., and Li, Y. (2019). Functional metal-organic frameworks for catalytic applications. Coord. Chem. Rev. *388*, 268–292.

40. Sun, Q., Tang, Y., Aguila, B., Wang, S., Xiao, F.S., Thallapally, P.K., Al-Enizi, A.M., Nafady, A., and Ma, S. (2019). Reaction environment modification in covalent organic frameworks for catalytic performance enhancement. Angew. Chem. Int. Ed. Engl. *58*, 8670–8675.

41. Acharjya, A., Pachfule, P., Roeser, J., Schmitt, F.J., and Thomas, A. (2019). Vinylene-linked covalent organic frameworks by base-catalyzed aldol condensation. Angew. Chem. Int. Ed. Engl. *58*, 14865–14870.

42. Cheng, K., Svec, F., Lv, Y., and Tan, T. (2019). Hierarchical micro-and mesoporous Zn-based metal-organic frameworks templated by hydrogels: their use for enzyme immobilization and catalysis of Knoevenagel reaction. Small *15*, 1902927.

43. Drout, R.J., Robison, L., and Farha, O.K. (2019). Catalytic applications of enzymes encapsulated in metal-organic frameworks. Coord. Chem. Rev. *381*, 151–160.

44. Chen, K., and Wu, C.D. (2019). Transformation of metal-organic frameworks into stable organic frameworks with inherited skeletons and catalytic properties. Angew. Chem. Int. Ed. Engl. *58*, 8119–8123.

45. Zhang, H., Li, G., Liao, C., Cai, Y., and Jiang, G. (2019). Bio-related applications of porous organic frameworks (POFs). J. Mater. Chem. B Mater. Biol. Med. *7*, 2398–2420.

46. Teplensky, M.H., Fantham, M., Li, P., Wang, T.C., Mehta, J.P., Young, L.J., Moghadam, P.Z., Hupp, J.T., Farha, O.K., Kaminski, C.F., and Fairen-Jimenez, D. (2017). Temperature treatment of highly porous zirconium-containing metal-organic frameworks extends drug delivery release. J. Am. Chem. Soc. *139*, 7522–7532.

47. Navarro-Sánchez, J., Argente-García, A.I., Moliner-Martínez, Y., Roca-Sanjuán, D., Antypov, D., Campíns-Falcó, P., Rosseinsky, M.J., and Martí-Gastaldo, C. (2017). Peptide metal-organic frameworks for enantioselective separation of chiral drugs. J. Am. Chem. Soc. *139*, 4294–4297.

48. Corella-Ochoa, M.N., Tapia, J.B., Rubin, H.N., Lillo, V., González-Cobos, J., Núñez-Rico, J.L., Balestra, S.R.G., Almora-Barrios, N., Lledós, M., Güell-Bara, A., et al. (2019). Homochiral metal-organic frameworks for enantioselective separations in liquid chromatography. J. Am. Chem. Soc. *141*, 14306–14316.

49. Zhang, S., Zheng, Y., An, H., Aguila, B., Yang, C.X., Dong, Y., Xie, W., Cheng, P., Zhang, Z., Chen, Y., and Ma, S. (2018). Covalent organic frameworks with chirality enriched by biomolecules for efficient chiral separation. Angew. Chem. Int. Ed. Engl. *57*, 16754–16759.

50. Liu, X., Huang, D., Lai, C., Zeng, G., Qin, L., Wang, H., Yi, H., Li, B., Liu, S., Zhang, M., et al. (2019). Recent advances in covalent organic frameworks (COFs) as a smart sensing material. Chem. Soc. Rev. *48*, 5266–5302.

51. Li, H.-Y., Zhao, S.-N., Zang, S.-Q., and Li, J. (2020). Functional metal-organic frameworks as effective sensors of gases and volatile compounds. Chem. Soc. Rev. *49*, 6364–6401.

52. Koo, W.-T., Jang, J.-S., and Kim, I.-D. (2019). Metal-organic frameworks for chemiresistive sensors. Chem *5*, 1938–1963.

53. Lustig, W.P., Mukherjee, S., Rudd, N.D., Desai, A.V., Li, J., and Ghosh, S.K. (2017). Metal-organic frameworks: functional luminescent and photonic materials for sensing applications. Chem. Soc. Rev. *46*, 3242–3285.

54. Wang, B., Lin, R.-B., Zhang, Z., Xiang, S., and Chen, B. (2020). Hydrogen-bonded organic Frameworks as a tunable Platform for functional materials. J. Am. Chem. Soc. *142*, 14399–14416.

55. Zhou, H.-C., Long, J.R., and Yaghi, O.M. (2012). Introduction to metal-organic frameworks. Chem. Rev. *112*, 673–674.

56. Zhang, X., Chen, Z., Liu, X., Hanna, S.L., Wang, X., Taheri-Ledari, R., Maleki, A., Li, P., and Farha, O.K. (2020). A historical overview of the activation and porosity of metal-organic frameworks. Chem. Soc. Rev. *49*, 7406–7427.

57. Feng, X., Ding, X., and Jiang, D. (2012). Covalent organic frameworks. Chem. Soc. Rev. *41*, 6010–6022.

58. Beuerle, F., and Gole, B. (2018). Covalent organic frameworks and cage compounds: design and applications of polymeric and discrete organic scaffolds. Angew. Chem. Int. Ed. Engl. *57*, 4850–4878.

59. Diercks, C.S., and Yaghi, O.M. (2017). The atom, the molecule, and the covalent organic framework. Science *355*, 923.

60. Zhang, K.-D., Tian, J., Hanifi, D., Zhang, Y., Sue, A.C.-H., Zhou, T.-Y., Zhang, L., Zhao, X., Liu, Y., and Li, Z.-T. (2013). Toward a single-layer two-dimensional honeycomb supramolecular organic framework in water. J. Am. Chem. Soc. *135*, 17913–17918.

61. Patil, R.S., Banerjee, D., Zhang, C., Thallapally, P.K., and Atwood, J.L. (2016). Selective CO_2 adsorption in a supramolecular organic framework. Angew. Chem. Int. Ed. Engl. *55*, 4523–4526.

62. Li, Y., Dong, Y., Miao, X., Ren, Y., Zhang, B., Wang, P., Yu, Y., Li, B., Isaacs, L., and Cao, L. (2018). Shape-controllable and fluorescent supramolecular organic frameworks through aqueous host–guest complexation. Angew. Chem. Int. Ed. *130*, 737–741.

63. Wang, H., Li, B., Wu, H., Hu, T.-L., Yao, Z., Zhou, W., Xiang, S., and Chen, B. (2015). A flexible microporous hydrogen-bonded organic framework for gas sorption and separation. J. Am. Chem. Soc. *137*, 9963–9970.

64. Karmakar, A., Illathvalappil, R., Anothumakkool, B., Sen, A., Samanta, P., Desai, A.V., Kurungot, S., and Ghosh, S.K. (2016). Hydrogen-bonded organic frameworks (HOFs): a new class of porous crystalline proton-conducting materials. Angew. Chem. Int. Ed. Engl. *55*, 10667–10671.

65. He, Y., Xiang, S., and Chen, B. (2011). A microporous hydrogen-bonded organic framework for highly selective C_2H_2/C_2H_4 separation at ambient temperature. J. Am. Chem. Soc. *133*, 14570–14573.

66. Hu, F., Liu, C., Wu, M., Pang, J., Jiang, F., Yuan, D., and Hong, M. (2017). An ultrastable and easily regenerated hydrogen-bonded organic molecular framework with permanent porosity. Angew. Chem. Int. Ed. Engl. *56*, 2101–2104.

67. Lin, R.-B., He, Y., Li, P., Wang, H., Zhou, W., and Chen, B. (2019). Multifunctional porous hydrogen-bonded organic framework materials. Chem. Soc. Rev. *48*, 1362–1389.

68. Li, P., He, Y., Zhao, Y., Weng, L., Wang, H., Krishna, R., Wu, H., Zhou, W., O'Keeffe, M., Han, Y., and Chen, B. (2015). A rod-packing microporous hydrogen-bonded organic framework for highly selective separation of C_2H_2/CO_2 at room temperature. Angew. Chem. Int. Ed. Engl. *54*, 574–577.

69. Wang, B., He, R., Xie, L.-H., Lin, Z.-J., Zhang, X., Wang, J., Huang, H., Zhang, Z., Schanze, K.S., Zhang, J., et al. (2020). Microporous hydrogen-bonded organic framework for highly efficient turn-up fluorescent sensing of aniline. J. Am. Chem. Soc. *142*, 12478–12485.

70. Feng, S., Shang, Y., Wang, Z., Kang, Z., Wang, R., Jiang, J., Fan, L., Fan, W., Liu, Z., Kong, G., et al. (2020). Fabrication of a hydrogen-bonded organic framework membrane through solution processing for pressure-regulated gas separation. Angew. Chem. Int. Ed. Engl. *59*, 3840–3845.

71. Hisaki, I., Ikenaka, N., Gomez, E., Cohen, B., Tohnai, N., and Douhal, A. (2017). Hexaazatriphenylene-based hydrogen-bonded organic framework with permanent porosity and single-crystallinity. Chemistry *23*, 11611–11619.

72. Yan, W., Yu, X., Yan, T., Wu, D., Ning, E., Qi, Y., Han, Y.-F., and Li, Q. (2017). A triptycene-based porous hydrogen-bonded organic framework for guest incorporation with tailored fitting. Chem. Commun. (Camb.) *53*, 3677–3680.

73. Li, P., He, Y., Arman, H.D., Krishna, R., Wang, H., Weng, L., and Chen, B. (2014). A microporous six-fold interpenetrated hydrogen-bonded organic framework for highly selective separation of C_2H_4/C_2H_6. Chem. Commun. (Camb.) *50*, 13081–13084.

74. Hisaki, I., Ikenaka, N., Tsuzuki, S., and Tohnai, N. (2018). Sterically crowded hydrogen-bonded hexagonal network frameworks. Mater. Chem. Front. *2*, 338–346.